Available online at www.sciencedirect.com
SCIENCE DIRECT
Journal of Catalysis 239 (2006) 340–346
JOURNAL OF CATALYSIS
www.elsevier.com/locate/jcat

Synergy of $Fe_xCe_{1-x}O_2$ mixed oxides for N_2O decomposition

F.J. Perez-Alonso [a], I. Melián-Cabrera [b,*], M. López Granados [a], F. Kapteijn [c,*], J.L.G. Fierro [a,*]

[a] *Instituto de Catalisis y Petroleoquımica, CSIC, Marie Curie 2, Cantoblanco, 28049 Madrid, Spain*
[b] *Stratingh Institute of Chemistry and Chemical Engineering, University of Groningen, Nijenborgh 4, 9747 AG Groningen, The Netherlands*
[c] *R&CE, DelftChemTech, Delft University of Technology, Julianalaan 136, 2628 BL Delft, The Netherlands*

Received 10 November 2005; revised 10 February 2006; accepted 13 February 2006

Available online 13 March 2006

Abstract

Fe–Ce mixed oxides prepared by coprecipitation showed considerable synergy in N_2O decomposition when compared with pure metal oxide counterparts. The mixed system also displayed higher stability in reaction at high temperature. Through characterisation by XRD, XPS and TPR, the activity–stability improvement is ascribed to the formation of Fe-doped ceria and Ce-doped hematite and also to increased surface area. The intimate interaction in the mixed phases results in easier reduction. Thus the release of oxygen, which is the rate-determining step in this N_2O decomposition, becomes more facile.

Keywords: Ceria; Iron catalysts; Co-precipitation; Hematite; N_2O decomposition

1. Introduction

Ceria-based catalysts display a wide range of applications, including vehicle exhaust gas emission control, electrolytes for solid oxide fuel cells (SOFCs), and catalysts for various oxidation and hydrogenation reactions [1–3]. For most of these applications, ceria-based oxides act as promoters of the active ingredient (or metal oxides) with which they are in close contact [1]. Depending on the type of reaction and the experimental conditions, different promoting effects, including structural, redox states, and bifunctional promotion, have been proposed to account for the synergetic effects observed [1]. Ceria-based mixed oxides $(Ce_xM_{1-x})O$ are versatile solid oxygen exchangers. At temperatures in the range of 400–800 °C, the redox couple $Ce^{IV} \leftrightarrow Ce^{III}$ facilitates oxygen storage and release from its bulk fluorite lattice, making it an ideal candidate for catalytic and/or electrocatalytic oxidation applications in SOFCs [3]. However, the *surface* redox chemistry of ceria is sensitive even at low temperatures to crystal structure defects [4], which can be tuned by substituting some of the Ce cations with ions of different sizes and/or charges [5]. Substitution of a lower-valent metal ion (e.g., M^{III}) by cerium lowers the energy barrier for oxygen migration [6]. However, smaller homovalent ions (Zr^{IV}) enhance the oxygen storage capacity (OSC) by decreasing the activation energy for the reduction ($Ce^{IV} \rightarrow Ce^{III}$) and retarding OSC degradation at high temperature. Given the effects of trivalent ions and smaller sizes on the structure and properties [7,8], there is considerable scientific interest in introducing M^{III} ions into the ceria lattice.

Ceramic methods allow the formation of such solid solutions, but the preparation temperature and time required to obtain a homogeneous mixture depends to a significant extent on the particle size of the starting material. Alternatively, we have recently shown that controlled coprecipitation results in a simpler method for achieving intimate mixing of Fe and Ce oxides [9]. The Fe–Ce interaction seems to occur through the formation of hematite-like and cubic ceria-like solid solutions. In the hematite-like solid solution, Ce cations are dissolved in the hematite structure, whereas Fe cations are dissolved in the cubic ceria structure. Such interactions were absent in samples prepared by physical mixing.

As far as catalytic applications are concerned, pure hematite (α-Fe_2O_3) or ceria (c-CeO_2) are not very active for N_2O decomposition [10]. For this reaction, the best catalyst is prepared

* Corresponding authors.
E-mail addresses: i.v.melian.cabrera@rug.nl (I. Melián-Cabrera), f.kapteijn@tnw.tudelft.nl (F. Kapteijn), jlgfierro@icp.csic.es (J.L.G. Fierro).

0021-9517/$ – see front matter
doi:10.1016/j.jcat.2006.02.008

by exchanging Fe^{III}/Fe^{II} salts (solid and gas) within a zeolite matrix, giving rise to high turnover rates even for low Fe loadings (ca. 0.5 wt% Fe) [11–15]. In this paper we show that Fe–Ce mixed oxides yield improved N_2O decomposition, much greater than those of the individual phases. Such a noticeable synergy is interpreted in terms of structural information derived from physicochemical analysis.

2. Experimental

2.1. Catalyst preparation

A series of coprecipitated iron-cerium oxide catalysts with 100, 95, 85, 50, and 0 at% Fe metal (Ce balance) was prepared by batchwise coprecipitation under vigorous stirring from 1 M aqueous solutions of $Fe(NO_3)_3{\cdot}9H_2O$ (Fluka, p.a. 98–101%) and $Ce(NO_3)_3{\cdot}6H_2O$ (Aldrich 99.99%), with a 5.6 M NH_4OH solution. Both solutions were simultaneously added at a constant rate of 50 mL/h by a perfusion pump (Becton Dickinson SE 400) to a precipitating batch containing 500 mL of distilled water at the start. The addition of the precipitating agent (NH_4OH) was accomplished using a pH-stationary device (Radiometer Copenhagen; ABU91 Autoburette), maintaining the pH constant at 8.0 during precipitation. Temperature was kept at 343 K. The precipitate thus obtained was aged for 16 h with the mother liquor still under stirring at the reaction temperature, with pH maintained at 8.0. Then the precipitate was filtered out and washed with successive portions of 400 mL of distilled water at 323 K. The precipitates were dried in air at 333 K for 24 h. These solids are referred to as Fe100Ce0 (pure Fe), Fe95Ce5, Fe85Ce15, Fe50Ce50, and Fe0Ce100 (pure Ce).

2.2. Characterisation techniques

Powder X-ray diffraction (XRD) patterns were recorded in the 5–80° 2θ range in scan mode (0.02°, 2 s) using a Seifert 3000 XRD diffractometer equipped with a PW goniometer with Bragg–Brentano $\theta/2\theta$ geometry, an automatic slit, and a bent graphite monochromator. The unit cell parameters were obtained by refining the peak positions of the XRD patterns with a least squares refinement method using the CELREF program [16]. To determine peak positions, the peak profiles were fitted with the commercially available ANALYZE program (pseudo-Voigt function). Thermoanalytical measurements were carried out on Perkin-Elmer TGA7 and DTA-7 devices. The experiments were carried out with ca 50 mg of sample, under air flow, 60 $ml_N\,min^{-1}$, and a heating rate of 10 $K\,min^{-1}$ in the 303–1273 K range. Nitrogen adsorption isotherms were obtained at the temperature of liquid nitrogen (77 K), using a Micromeritics ASAP 2000 apparatus. Samples were degassed at 413 K for 12 h before the adsorption isotherm was determined. BET areas were computed from the adsorption isotherms ($0.05 < P/P_0 < 0.30$), taking a value of 0.164 nm^2 for the cross-section of the adsorbed N_2 molecule at 77 K.

Hydrogen temperature-programmed reduction (H_2-TPR) was carried out in a U-shaped quartz reactor connected to a QMS 200 Balzers Prisma quadrupole mass spectrometer for on-line gas analysis. The sample (50 mg) consisted of solid particles in the 250–300 μm range. The gas flow rate was 50 $ml_N\,min^{-1}$ (10% vol. H_2/Ar), and the heating rate was 10 $K\,min^{-1}$ (298–1073 K). The fragments $m/z = 2$ (H_2) and $m/z = 18$ (H_2O) were continuously monitored. Gas lines from the reactor to the inlet of the mass spectrometer were heated to 393 K to avoid water condensation. Quantification of the water signal was done through a calibration curve obtained with a high-purity CuO (99.9999%, Aldrich).

X-Ray photoelectron spectroscopy (XPS) was done with a VG Escalab 200R spectrometer equipped with a hemispherical electron analyzer and an Al-K_α ($h\nu = 1486.6$ eV) X-ray source. The samples were outgassed at room temperature within the pretreatment chamber of the spectrometer. Several pretreatments were performed to evaluate the effect of N_2O exposure. These involved heating up in helium at 823 K and N_2O exposure (4.5 mbar in He) at the same temperature. The binding energies of Ce 3d, Fe 2p, and C 1s core levels were determined, referencing to the binding energy of adventitious C 1s signal at a binding energy of 284.9 eV, which gives an accuracy of ±0.1 eV. Peak intensities were estimated by calculating the integral of each peak, after smoothing, subtracting an S-shaped (Shirley) background, and fitting the experimental curve to Lorentzian and Gaussian lines of variable proportion. Atomic ratios were then computed from the intensity ratios normalised by atomic sensitivity factors.

2.3. N_2O-decomposition activity tests

The activity measurements were carried out in a six-flow reactor [17] using 50 mg of precursor (particle size 250–300 μm). The following conditions were applied: 4.5 mbar N_2O (balanced with He), 3 bar-a total pressure, and temperature range of 473–873 K at GHSV = ∼23,800 h^{-1}. Before the reaction, the precursor was activated both in He and air (flow of 50 $mL\,min^{-1}$) at 873 K (at a heating rate of 5 $K\,min^{-1}$) for 1 h. The reactor effluents were analysed by gas chromatography (Chrompack CP 9001) after 1 h reaction at each temperature. This time assured that the measurements were obtained under steady-state conditions for every temperature. Note that the space velocity used (GHSV = ∼23,800 h^{-1}) was somewhat lower than that commonly used for Fe zeolites (>40,000 h^{-1}); low velocities were required to show substantial activity for this sort of catalyst in the range of 673–873 K.

3. Results and discussion

3.1. Activity results

The conversion of N_2O as a function of the reaction temperature is shown in Fig. 1. All of the catalysts showed substantial activity in the temperature range studied. The onset of the conversion occurred at around 623 K for the most active catalyst.

The mixed Fe–Ce catalysts were significantly more active than the pure Fe100Ce0 and Fe0Ce100 catalysts. The enhancement of activity at a certain temperature increased with increasing Ce content in the series. This effect can also be inter-

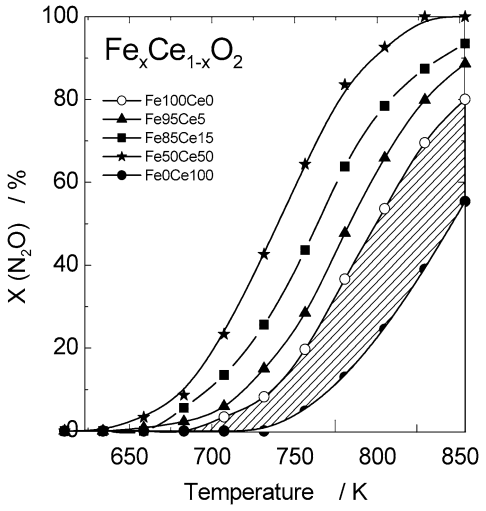

Fig. 1. N_2O conversion vs. temperature for different Fe–Ce catalysts. The dashed area would correspond to physical mixtures Fe–Ce (i.e., additive effect of CeO_2 and FeO_x). Conditions: 4.5 mbar N_2O, balance He, $P = 3$ bar, GHSV = 23,800 h^{-1}.

preted as a shift to lower operation temperatures at a constant conversion. The optimal performance was achieved with the Fe50Ce50 catalyst, reaching full conversion at 823 K. A closer analysis of the conversion curves clearly shows that the effect of CeO_2 was not due to an additive effect of both phases. This would imply that the activity for the mixed Fe–Ce catalysts lies between the Fe100Ce0 and Fe0Ce100 curves (dashed area in Fig. 1). The addition of CeO_2 by coprecipitation gives rise to a synergetic effect between Fe and Ce.

The stability of the catalysts was studied by testing the activity during the cooling step after the maximum temperature (873 K) was reached. As an example, Fig. 2 plots the heating and cooling activity branches for the Fe100Ce0 and Fe50Ce50 catalysts. The Fe100Ce0 system showed loss of activity. The sample was not stable to high-temperature treatments under reaction conditions. This loss may be related to deactivation by thermal sintering of the FeO_x domains. This idea is supported by the BET area study. The Fe100Ce0 precursor was calcined at different temperatures, and the BET was measured by N_2 physisorption. It was found that the BET area changed from 26.7 $m^2\,g^{-1}$ (573 K) to 13.9 $m^2\,g^{-1}$ (773 K) and, finally, to 7.5 $m^2\,g^{-1}$ at 873 K (pretreatment temperature and highest reaction temperature). In contrast, the Fe50Ce50 catalyst showed no loss of activity during cooling, and BET area decreased in a lower proportion, from 79.3 $m^2\,g^{-1}$ (573 K) to 50.8 $m^2\,g^{-1}$ (773 K) and, finally, to 28.0 $m^2\,g^{-1}$ at 873 K. It is clear that the mixed oxide formation results in a more stable solid against sintering processes. In addition, calcination variants, such using He or air, did not show differences in terms of activity and stability of the final phases. A slight induction time was observed when the catalysts were calcined in air (data not shown).

The data shown in Fig. 1 refer to the fresh catalysts dried at 333 K and loaded into the reactor. These samples were pretreated in situ in He at 823 K before the reaction. Thermogravimetric analysis revealed that the samples lose weight at such temperatures. Thus the "weight basis" for every catalyst

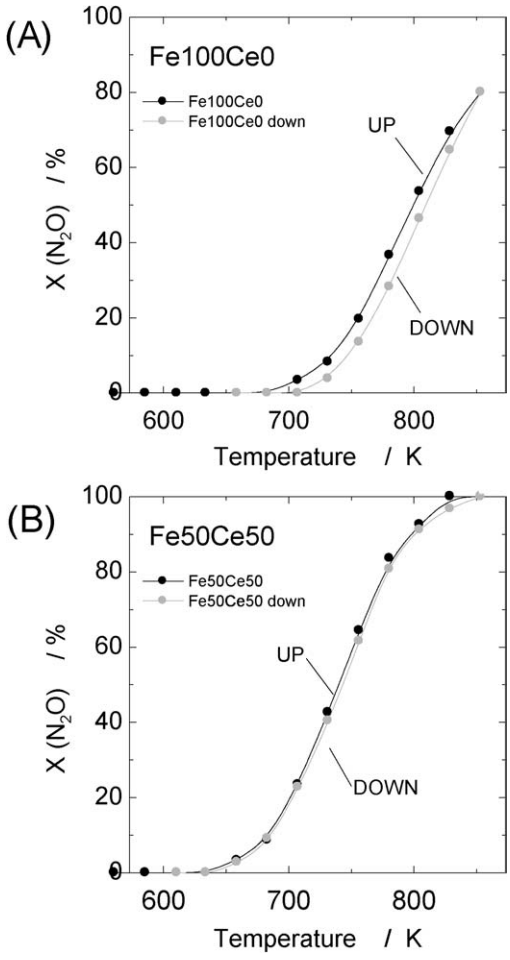

Fig. 2. Stability study of the catalysts by cooling down in the reaction mixture (grey branch). (A) Pure Fe sample (Fe100Ce0), (B) equimolar molar Fe50Ce50 sample.

Table 1
Weight lost of the different catalysts after calcination at 873 K and specific BET areas derived from N_2 physisorption of samples calcined at same temperature

Catalyst	Weight loss (TGA) (%)	BET ($m^2\,g^{-1}$)
Fe100Ce0	19.3	7.5
Fe95Ce5	13.7	21.0
Fe85Ce15	25.8	32.0
Fe50Ce50	25.2	28.0
Fe0Ce100	2.5	12.3

could be different just before the reaction, and the data have been corrected for this. The weight losses at 823 K in He for the catalyst precursors are given in Table 1. The loss in weight depends on the composition and is not negligible. To normalize data, the conversion rate was also calculated based on the "true" weight. Fig. 3A shows the apparent N_2O conversion rate at 773 K as μmol/(s kg). Two rate series are compared, one based the weight of the fresh dried catalyst (gray columns) and the other (black bars) based on the sample weight just before the reaction (Table 1). The synergetic effect of the mixed oxide is apparent for both approaches, but even more pronounced with the corrected sample weights.

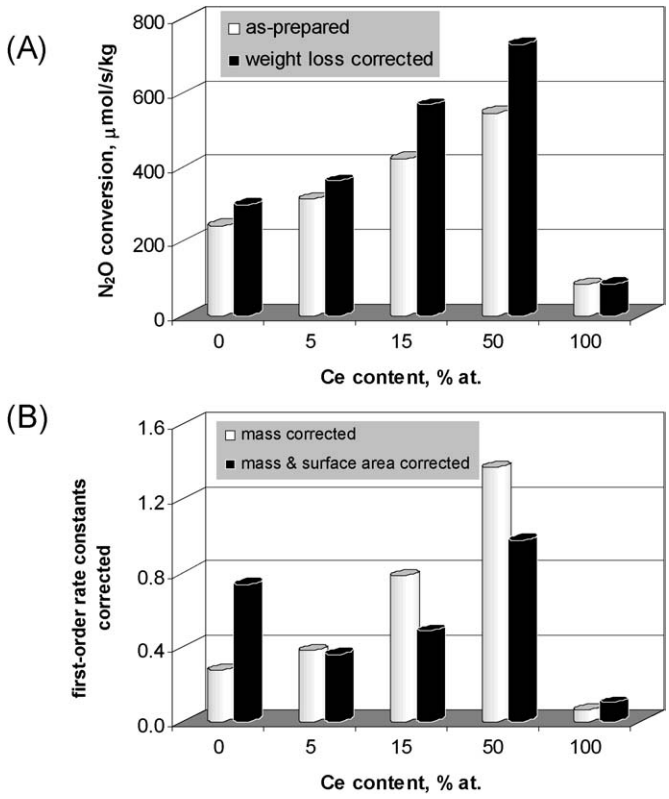

Fig. 3. (A) N_2O conversion at 773 K as µmol/(s kg) as a function of the Ce content. Two series are given. The first one is referred to the fresh catalyst weight basis (grey bars), while the other one comprises the weight loss correction due to pretreatment temperature (823 K) just before the reaction. Conditions: same as in Fig. 1. (B) Representation of the first-order rate constants (estimate) per unit corrected mass (grey) and per unit surface area (black). The latter values were multiplied by 20 for scaling.

In summary, mixtures of Fe–Ce obtained by coprecipitation gave rise to a synergetic effect in N_2O decomposition.

3.2. Mixed oxides formation

Fig. 3 shows DTA profiles for the precursor samples. The featureless DTA trace of the Fe0Ce100 sample is consistent with its fluorite-type CeO_2 structure derived from the XRD pattern of the precursor (Fig. 4). All the Fe-containing samples show a weak endothermic peak at ca. 475 K, associated with desorption of weakly adsorbed water, together with a strong exothermic peak at 525 K. In agreement with previous reports [18,19], this latter peak has been ascribed to water produced through transformation of ferrihydrite into crystalline α-Fe_2O_3 (hematite).

This peak is weaker in the Fe95Ce5 sample (and located at 550 K) but clearly visible in the rest of the Fe-containing samples, suggesting that ferrihydrite or related phase was present in the precursors of the samples. The experimental conditions under which precipitation was carried out favour the formation of amorphous ferrihydrite versus goethite [18]. On the other hand, two differences can be detected between pure Fe and coprecipitated Fe–Ce samples. First, a broad exothermic peak is seen in the DTA profile for the 100Fe sample at 710 K, reportedly caused by the crystallisation of ill-crystallised anhydrous Fe^{III} oxide to crystalline α-Fe_2O_3. This appears while NO_x is released from the thermal decomposition of the rest of nitrates still left adsorbed on the ferrihydrite [20]. Indeed, nitrogen oxides were observed by mass spectrometry analysis (not shown). This feature at 710 K is not detected in the Fe–Ce–O precursors, indicating the particular nature of the coprecipitated samples. Another remarkable feature of the Fe–Ce DTA curves is the remarkably strong exothermic peak at ca. 930 K associated to phase change of Fe–Ce–O. According to characterisation results (XRD, Raman, and Mössbauer spectroscopy) reported previously [9], this peak represents the segregation of c-CeO_2 and α-Fe_2O_3 from the mixed oxides. Based on the DTA findings, the stability of the Fe–Ce–O mixed oxides formed would be ensured until 930 K.

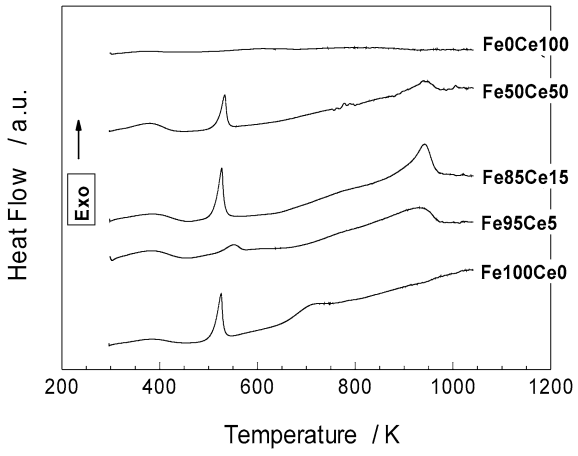

Fig. 4. DTA results of precursors. Conditions: flow of air (60 mL_N/min), ramping rate: 10 K/min.

This finding was verified by XRD. Fig. 5A shows the X-ray difractograms of the samples after pretreatment at 873 K before reaction. The reflections can be assigned either to hematite, α-Fe_2O_3 (hexagonal, R-3c) [18] or cubic CeO_2 (fluorite structure, Fm3m) [21]. In the Fe100Ce0 sample, only α-Fe_2O_3 reflections were observed (marked as ▼), whereas in the Fe0Ce100 sample, those of c-CeO_2 (■) were seen.

The mixed Fe95Ce5, Fe85Ce15, and Fe50Ce50 samples displayed reflections from both phases. Decreased intensity was observed in the reflections from α-Fe_2O_3 and c-CeO_2 with increased Ce and Fe concentration in the samples, respectively. Moreover, they were wider than for the pure Fe and Ce samples, which can be taken as evidence of smaller crystal size and/or microstrain [22]. It was observed that c-CeO_2 peaks from Fe–Ce–O samples shift toward higher diffraction angles (see the detail in Fig. 5C). To test whether or not solid solutions were formed, unit cell parameters were calculated from the Bragg angles. Unit cell parameters for each structure are collected in Table 2. In the Fe95Ce5 sample, the low intensity of the c-CeO_2 reflections observed did not allow accurate determination of the unit cell parameters of this structure.

A contraction of the unit cell for c-CeO_2 structure was observed for Fe85Ce15 and Fe50Ce50 with respect to pure Ce. This indicates that c-CeO_2-like solid solutions were formed in

Table 2
Unit cell parameters of the phases detected in the different samples as determined by CELREF

	CeO_2			
	Fe0Ce100	Fe50Ce50	Fe85Ce15	
a (Å)	5.4111 ±0.0002	5.3852 ±0.0076	5.3656 ±0.0158	
	α-Fe_2O_3			
	Fe100Ce0	Fe95Ce5	Fe85Ce15	Fe50Ce50
a (Å)	5.0351 ±0.0009	5.0363 ±0.0013	5.0388 ±0.0020	5.0429 ±0.0009
c (Å)	13.7453 ±0.0002	13.7592 ±0.0002	13.7644 ±0.0006	13.7651 ±0.0012

which Ce^{IV} is substituted by Fe^{III}. The contraction is due to the smaller size of the Fe^{III} cation (0.64 Å) [18] compared to the Ce^{IV} cation (1.01 Å) [21] inside the *c*-CeO_2 structure. XRD also showed that as the Ce proportion rises, the peaks from the ceria solid solution become more intense, indicating that the concentration of the Fe-doped ceria-like structure increases with increasing Ce content.

In terms of the hematite phase, the reflections were also seen with increasing Ce content. A shift toward lower reflection angles was observed, although much smaller (but visible) than those observed for the CeO_2 (Fig. 5B). Indeed, the unit cell parameters of the hematite showed a trend with increasing Ce, particularly in the parameter *c*. This can be interpreted as incorporation of Ce^{IV} in the hematite structure, leading to an expansion of the unit cell. The charge neutrality could be achieved as substitution of part of O^{2-} by OH^-, which also produces an expansion of the structure as was reported by Schwertmann et al. [23]. In summary, analysis of the unit cell parameters and diffraction profiles showed that Fe–Ce–O solid solutions with a *c*-CeO_2-type structure and an α-Fe_2O_3 structure were formed.

In terms of apparent activity (Fig. 3A), the optimal performance was achieved with the Fe50Ce50 catalyst, which showed the largest proportion of ceria solid solution. Another important parameter to be studied is the porosity of the samples. N_2 isotherms were measured, and the BET values derived are collected in Table 1. The porosity of the mixed solid solutions is better than that of their pure oxide counterparts. The surface area also increased with increasing weight loss. The decomposition at high temperature creates void space. Fig. 3B shows a calculation of the first-order rate constants, corrected for mass and surface area. Normalization per mass (gray columns) is in agreement with Fig. 3A. On accounting for the specific surface (black bars), the original conclusion still holds for Fe50Ce50, although the pure Fe100Ce0 now shows a considerable increase in intrinsic kinetic terms. Therefore, the increased BET area of mixed systems influences catalyst performance, but is not the sole determining parameter. The most significant factor is the solid solution formation, because Fe50Ce50 (with the greatest solid solution formation) displays the optimal activity, even though it does not have the greatest BET area. Based on the activity trends, it is reasonable to propose that Fe doping in a ceria-type structure dominates the final catalytic performance. The larger the proportion of ceria-like solid solution found by XRD, the greater the catalytic effect; however, the participation of hematite-like solid solution cannot be completely ruled out.

3.3. Synergetic effect characterisation

Fig. 6 shows the hydrogen-TPR profile in terms of water formation. It is well documented that the reduction of bulk hematite (α-Fe_2O_3) proceeds via magnetite (Fe_3O_4) and wustite (FeO) to metallic iron. However, the formation of wustite cannot be observed because it is metastable and disproportionates into magnetite and metallic iron ($4FeO \rightarrow Fe_3O_4 + Fe$) below 893 K [24]. Fe100Ce0 shows characteristic features of hematite with a sharp peak at 638 K and a broad peak around 850 K, corresponding to the reduction of hematite to magnetite and of magnetite to Fe^0, respectively [25]. The Fe–Ce–O samples show similar, but more complex profiles involving more reduction peaks beyond 640 K as a consequence of the system's complex composition. However, the most important feature is

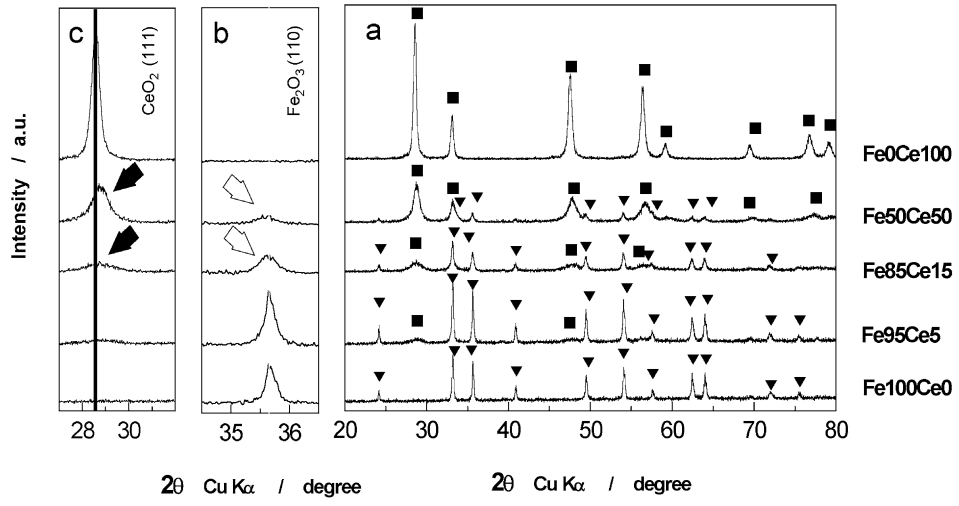

Fig. 5. (a) XRD patterns of the samples calcined at 873 K: (■) *c*-CeO_2, (▼) α-Fe_2O_3. (b) Amplification of the (110) reflection for α-Fe_2O_3 and (111) reflection for ceria in (c).

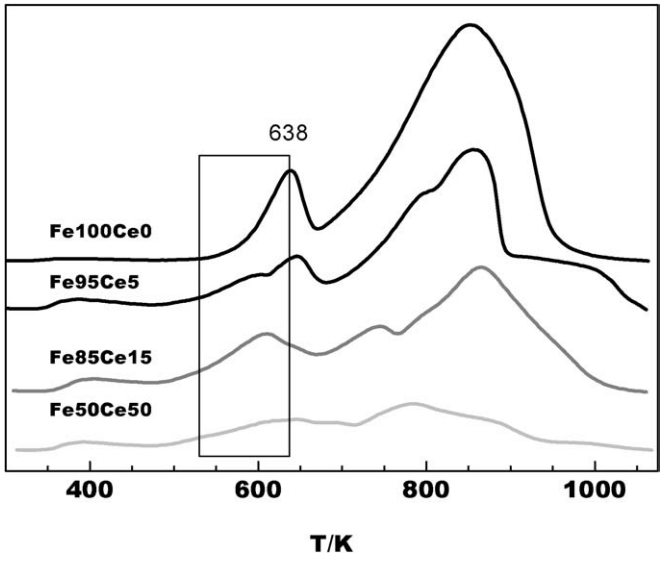

Fig. 6. TPR-H_2 (in terms of H_2O formation) of the different samples as referred in the graph. Conditions: 10% H_2/Ar, 50 mL_N/min and ramping rate of 10 K/min. Rectangle represents the reduction region of hematite to magnetite.

the enhanced reducibility related to the close interaction between Fe and Ce cations found in the precipitated samples. The addition of Ce shifts the peak of the hematite-to-magnetite reduction to lower temperatures.

This is clearly seen in the Fe50Ce50 sample, which shows the most pronounced promotion in N_2O decomposition. These observations are quite important, because N_2O decomposition is related to the reducibility of Fe species. The rate-determining step for such a reaction is the removal of adsorbed oxygen [26], a reductive step. This was recently demonstrated by means of TAP experiments for Fe zeolites [27]. The situation is similar for mixed oxides. Rothenberg et al. [28] showed that for ceria-doped systems, hydrogen is required to remove oxygen from the ceria structure at temperatures around 773 K; apparently, oxygen does not desorb on its own at those temperatures. Clearly, oxygen removal is a difficult step, as is N_2O decomposition of oxides. Therefore, the better the reducibility of the Fe sites, the better the catalyst performance. This correlation with TPR is also found for Fe zeolites [29]; it was shown that Fe-FER zeolite is the optimal system for this reaction, showing higher reducibility than Fe-BEA and Fe-ZSM5 zeolites.

Preliminary XPS measurements were carried out to investigate the synergetic effect. Fe 2p levels did were not significantly different among the samples. However, Ce 3d emission displayed a special feature. Fig. 7 gives the Ce 3d core-level spectra for two samples, optimal Fe50Ce50 and pure Ce. A qualitative estimation of the degree of reduction of Ce^{IV} oxide can be made based on the valley defined by the V and V″ features of the spectrum (Fig. 6). If Ce oxide contains only a small amount of Ce^{III}, then the valley is very well defined, but if the degree of reduction of Ce^{IV} to Ce^{III} is high, then Ce^{III} becomes more concentrated, the V′ feature of Ce^{III} becomes more intense, and the valley between V and V″ starts to vanish [30–36]. When the samples were treated in an N_2O/He mixture (4.5 mbar in N_2O in situ before the measurement) at 873 K, after pretreatment in He at the same temperature, the valley between V and V″ was much less well defined for Fe50Ce50. This indicates that Ce^{III} is not oxidized by the effect of N_2O treatment. Conversely, this effect was not observed for Fe0Ce100. This can be interpreted

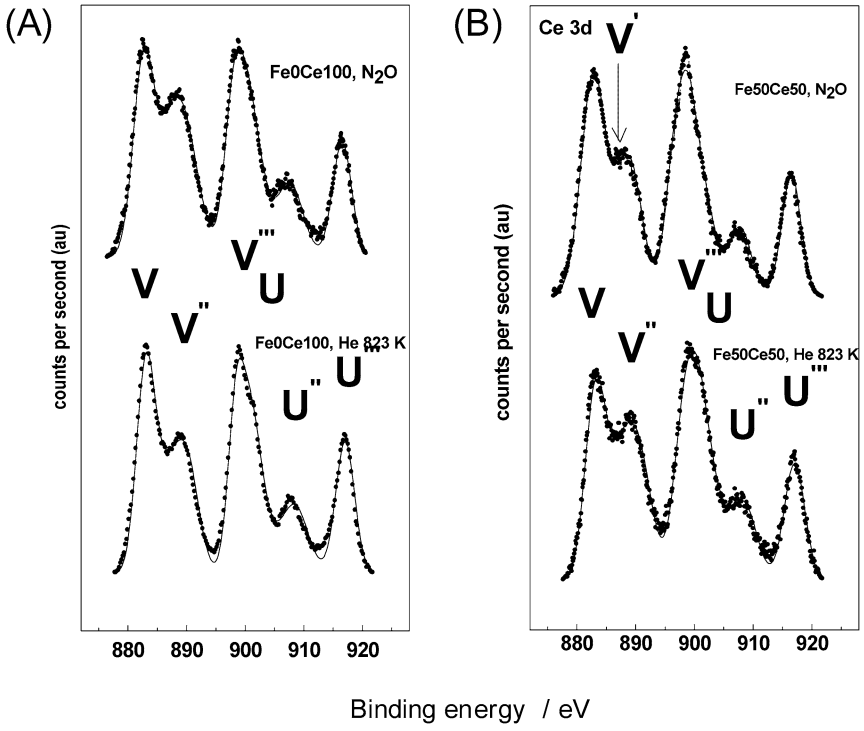

Fig. 7. XPS spectra of the Ce 3d core level at two pretreatment conditions, Helium at 823 K and after exposure of N_2O (4.5 mbar N_2O, He balance). (A) Fe0Ce100 and (B) Fe50Ce50 catalysts.

by assuming that Ce^{III}, and thus oxygen vacancies, are generated more readily during treatment with He in the Fe50Ce50 catalyst. N_2O is more easily decomposed; therefore, the oxygen deposited by N_2O is less stable (more reactive) in the mixed system compared with the pure oxide, resulting in enhanced oxygen desorption, which is the rate-determining step for N_2O decomposition. This explains the higher activity for the mixed system, although the chemical explanation of the synergetic effect through the doping has not yet been elucidated. Based on the present results, Fe–Ce–O solid solutions (Fe, 5–50 mol%) are promising for improved N_2O decomposition catalysts. Future studies are needed to evaluate the synergetic effect in the presence of other components such as NO, O_2, and H_2O.

4. Conclusion

Simultaneous precipitation of Ce^{IV} and Fe^{III} nitrates with ammonia, along with calcination at 873 K, leads to Fe–Ce–O mixed oxides. A noticeable synergetic effect was observed for the activity in N_2O decomposition when compared with the pure metal oxide catalysts. This synergetic effect can be attributed to the formation of a Fe–ceria-like solid solution and a Ce–hematite-like solid solution. The improved specific areas of the mixed systems contribute to the better performance. Among the catalysts studied, Fe50Ce50 was the most active. Its higher proportion of Fe-doped ceria, although having a lower specific surface than Fe85Ce15, reinforces the hypothesis that it has the most active Fe environment. TPR showed that the addition of Ce improved the hematite-to-magnetite reduction by a shift to lower temperatures. This finding correlates very well with the N_2O decomposition performance. The reactivity was confirmed by XPS after pretreating the samples in He and treating them in N_2O afterward. The oxygen derived from N_2O decomposition is less stable (Ce^{IV} is partially reduced to Ce^{III}) in the mixed oxide system compared with the pure cases. Based on our findings, we conclude that Fe–Ce–O solid solutions (Fe, 5–50 mol%) are promising systems for improved N_2O decomposition catalysts.

Acknowledgments

This study was supported in part by grants from MCYT Spain (projects MAT2001-2215-C03-01 and ENE2004-07345-C03-01/ALT) and the European Commission (contract HPMF-CT-2002-01873). F.J.P.A. acknowledges a doctoral fellowship from MEC (Spain), and I.M.-C. thanks the European Commission (Marie Curie Actions) and Senter-Novem (NL) for a postdoctoral grant and funding, respectively.

Supplementary material

The online version of this article contains additional supplementary material.

Please visit doi:10.1016/j.jcat.2006.02.008.

References

[1] A. Trovarelli, Catal. Rev. Sci. Eng. 38 (1996) 439.
[2] E.P. Murray, T. Tsai, S.A. Barnett, Nature 400 (1999) 649.
[3] S. Park, J.M. Vohs, R.J. Gorte, Nature 404 (2000) 265.
[4] A.E.C. Palmqvist, M. Wirde, U. Gelius, M. Muhammed, Nanostruct. Mater. 11 (1999) 995.
[5] G. Rothenberg, E.A. de Graaf, A. Bliek, Angew. Chem., Int. Ed. 41 (2003) 3066.
[6] A. Trovarelli, Comments Inorg. Chem. 20 (1999) 263.
[7] G. Balducci, J. Kaspar, P. Fornasiero, M. Graziani, M.S. Islam, J. Phys. Chem. B 102 (1998) 557.
[8] E. Mamontov, T. Egami, R. Brezny, M. Koranne, S. Tiagi, J. Phys. Chem. B 104 (2000) 11110.
[9] F.J. Pérez-Alonso, M. López Granados, M. Ojeda, P. Terreros, S. Rojas, J.L.G. Fierro, M. Gracia, R. Gancedo, Chem. Mater. 17 (2005) 2329.
[10] F. Kapteijn, J. Rodriguez-Mirasol, J.A. Moulijn, Appl. Catal. B: Environ. 9 (1996) 25–64, and references therein.
[11] X.B. Feng, W.K. Hall, Catal. Lett. 41 (1997) 45.
[12] H.Y. Chen, W.M.H. Sachtler, Catal. Today 42 (1998) 73.
[13] G. Delahay, M. Mauvezin, A. Guzman-Vargas, B. Coq, Catal. Commun. 3 (2002) 385.
[14] J. Pérez-Ramirez, F. Kapteijn, K. Schöffel, J.A. Moulijn, Appl. Catal. B: Environ. 44 (2003) 117.
[15] J.A.Z. Pieterse, S. Booneveld, R.W. van den Brink, Appl. Catal. B: Environ. 51 (2004) 215.
[16] CELREF unit-cell refinement software for Windows by Laugier and Bochu, URL site: http://www.ccp14.ac.uk/.
[17] J. Pérez-Ramırez, R.J. Berger, G. Mul, F. Kapteijn, J.A. Moulijn, Catal. Today 60 (2000) 93.
[18] R.M. Cornell, U. Schwertmann, The Iron Oxides: Structure, Properties, Reactions and Uses, VCH Publishers, New York, 1996.
[19] Z. Fheng, J. Zhao, F.E. Huggins, G.P. Huffmann, J. Catal. 143 (1993) 510.
[20] J. Subrt, V. Stengl, M. Skokánek, Thermochim. Acta 211 (1992) 107.
[21] J. Kăspar, P. Fornasiero (Eds.), Catalysis by Ceria and Related Materials, Imperial College Press, London, 2002.
[22] G. Kimmel, D. Dayan, in: H.J. Bunge, R.L. Snyder, J. Fiala (Eds.), IUCR Monographs on Crystallography, vol. 10, Oxford Science Publications, 1999, pp. 698–727.
[23] E. Wolska, U. Schwertmann, Z. Kristallogr. 189 (1989) 223.
[24] Y. Jin, A.K. Datye, J. Catal. 196 (2000) 8.
[25] T.V. Voskoboinikov, H.Y. Chen, W.M.H. Sachtler, Appl. Catal. B: Environ. 19 (1998) 279.
[26] F. Kapteijn, J. Rodriguez Mirasol, J.A. Moulijn, Appl. Catal. B: Environ. 9 (1996) 25.
[27] J. Perez-Ramirez, F. Kapteijn, G. Mul, J.A. Moulijn, J. Catal. 208 (2002) 211.
[28] G. Rothenberg, E.A. de Graaf, A. Bliek, Angew. Chem. Int. Ed. 42 (2003) 3365.
[29] I. Melian-Cabrera, C. Mentruit, J.A.Z. Pieterse, R.W. van den Brink, G. Mul, F. Kapteijn, J.A. Moulijn, Catal. Commun. 6 (2005) 301.
[30] D.R. Mullins, S.H. Overbury, D.R. Huntley, Surf. Sci. 409 (1998) 307.
[31] M. Romeo, K. Bak, J. El Fallah, F. Le Normand, L. Hilaire, Surf. Interface Anal. 20 (1993) 508.
[32] M. Paulis, H. Peyrard, M. Montes, J. Catal. 199 (2001) 30.
[33] M. Daturi, C. Binet, J.C. Lavalley, A. Galtayries, R. Sporken, Phys. Chem. Chem. Phys. 1 (1999) 5717.
[34] B. Noronha, E.C. Fendley, R.R. Soares, W.E. Alvarez, D.E. Resasco, Chem. Eng. J. 82 (2001) 21.
[35] A.E. Hughes, J.D. Gorman, P.J.K. Patterson, R. Carter, Surf. Interface Anal. 24 (1996) 634.
[36] C. Larese, F. Cabello Galisteo, M. López Granados, R. Mariscal, J.L.G. Fierro, P.S. Lambrou, A.M. Efstathiou, J. Catal. 226 (2004) 443.